APPLIED SCIENCES AND ENGINEERING

Giant extraordinary transmission of acoustic waves through a nanowire

T. Devaux[1], H. Tozawa[1], P. H. Otsuka[1], S. Mezil[1], M. Tomoda[1], O. Matsuda[1], E. Bok[2], S. H. Lee[2], O. B. Wright[1]*

Wave concentration beyond the diffraction limit by transmission through subwavelength structures has proved to be a milestone in high-resolution imaging. Here, we show that a sound wave incident inside a solid over a diameter of 110 nm can be squeezed through a resonant meta-atom consisting of a nanowire with a diameter of 5 nm equal to $\lambda/23$, where λ is the incident acoustic wavelength, corresponding to a transmission efficiency of 500 or an energy densification of ~14,000. This remarkable level of extraordinary acoustic transmission is achieved in the absence of ultrasonic attenuation by connecting a tungsten nanowire between two tungsten blocks, the block on the input side being furnished with concentric grooves. We also demonstrate that these "solid organ pipes" exhibit Rayleigh end corrections to their effective longitudinal resonant lengths notably larger than their in-air analogs. Grooves on the output side lead to in-solid directed acoustic beams, important for nanosensing.

INTRODUCTION

Since the discovery of enhanced optical transmission through an array of subwavelength holes in a metal film, much work has been performed to study this effect and optimize it (1). Extraordinary transmission, i.e., the passage of more wave energy than expected by geometrical considerations through small subwavelength apertures, is a metamaterial-related phenomenon based on local resonances and is not confined to a particular wave type. After being demonstrated for electromagnetic waves (2), extraordinary acoustic transmission (EAT) was also subsequently shown to be possible (3). The acoustic case promises lower losses, higher performance and applications mirroring the optical case, for example, in acoustic focusing, imaging, or sensing. EAT was first demonstrated for bulk acoustic waves in liquid-solid and air-solid systems (3–8) by means of Fabry-Pérot (FP) or surface wave resonances in arrays of subwavelength holes or slits. Following on from progress in optics (9–11), coupling FP resonances in holes or slits with adjacent grooved architectures (12–15) was also shown to give rise to efficient transmission of bulk acoustic waves. In addition, geometries consisting of stacks of perforated plates (16) or systems with different fluids on either side of a perforated plate (17) have been shown to exhibit EAT. Likewise for metamaterials involving airborne sound with zero effective density based on the use of membranes (18, 19) or zero effective compressibility based on the use of Helmholtz resonators (20, 21), with transmission efficiencies up to ~100 (18, 19). However, although EAT has been demonstrated for surface acoustic waves on solids (22), it has not been demonstrated for bulk waves in solids, a geometry with potential applications in solid-state acoustic wave concentration and focusing. In contrast to the case of EAT involving fluids in which significant viscoelastic losses occur, record values of the transmission efficiency are expected for bulk waves in solids.

Here, we demonstrate extraordinary bulk-wave acoustic transmission inside a solid structure for the case of a tungsten nanowire,

acting as a gigahertz acoustic meta-atom, that is connected between two tungsten blocks. By including concentric grooves of optimal dimensions, we show how the EAT efficiency can be markedly increased to a value exceeding 500 for longitudinal waves and how directed output beams—similar to those found in fluid-solid systems (12, 14)—can be produced, a scalable result that should prove useful for future imaging and sensing applications.

RESULTS

Geometry and analysis

We study the case of a cylindrical tungsten nanowire (23–25) of length L = 40 nm and diameter d = 5 nm joining two tungsten blocks, as shown in Fig. 1 (A and E). We investigate the three generic geometries shown in Fig. 1 (B to D) by means of numerical simulations (see Materials and Methods): when no grooves are on the block surfaces, when concentric circular grooves are on the wave input side block, and when these circular grooves are on both the wave input and wave output side blocks.

The longitudinal wave energy spectrum $T(f)^2$ [where $T(f)$ is the amplitude transmission coefficient] is evaluated by integrating the Fourier modulus of the square of the acoustic dilatation over input and output analysis regions in the form of a disc and a hemispherical shell, respectively (see Fig. 1A and Materials and Methods). The transmission efficiency $\eta(f)$ is given by

$$\eta(f) = \frac{T^2(f)}{d^2/D^2} \tag{1}$$

where D is the diameter of the input analysis region and d^2/D^2 is the fraction of transmitted acoustic energy calculated on the basis of relative areas alone. The condition $\eta(f) > 1$ for a particular frequency f corresponds to a transmission that is greater than expected on the basis of relative areas, i.e., to EAT.

Case of no grooves

The results for the simulated transmission efficiency spectra are presented in Fig. 2. Figure 2A shows the transmission efficiency

[1]Division of Applied Physics, Faculty of Engineering, Hokkaido University, Sapporo 060-8628, Japan. [2]Institute of Physics and Applied Physics, Yonsei University, Seoul 03722, Republic of Korea.
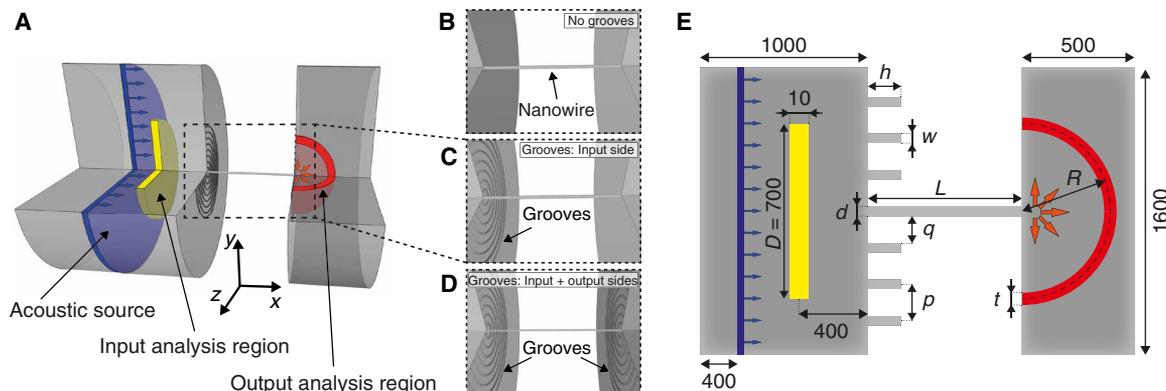*Corresponding author. Email: olly@eng.hokudai.ac.jp

Fig. 1. EAT architectures containing a nanowire with or without additional concentric grooves. (**A**) Schematic diagram of the EAT geometry, showing a section through a subwavelength-diameter tungsten nanowire connecting two tungsten half-spaces. Three different cases are considered: (**B**) case of no grooves, (**C**) case of grooves on the input side, and (**D**) case of grooves on both input and output sides. (**E**) Cross section for grooves on the input side with dimensions in nanometers. The acoustic source and analysis regions are also shown.
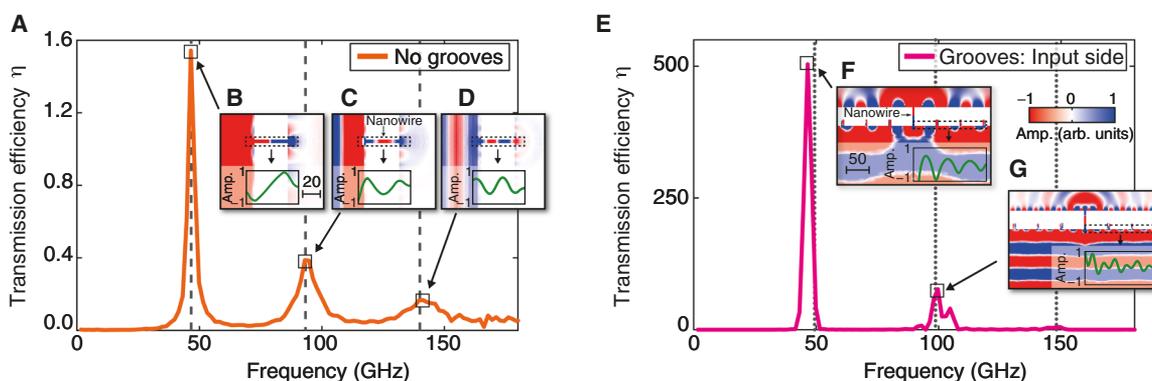

Fig. 2. Simulated spectra of the transmission efficiency η(f). The nanowire length is $L = 40$ nm and the radius is $a = 2.5$ nm. (**A**) η(f) for the case of no grooves, corresponding to Fig. 1B. Vertical dashed lines denote calculated FP resonances of the nanowire from Eq. 2 with end correction $\Delta L = 1.26a$ applied. (**B** to **D**) Associated x-y plane dilatation fields in the nanowire at the first three resonances together with dilatation-amplitude line plots sampled in the x direction averaged over the nanowire in the area delimited by the black dashed lines. (**E**) η(f) for the case of $N = 8$ grooves on the input side, corresponding to Fig. 1C. The groove dimensions are optimized. Vertical dotted lines denote calculated Rayleigh wave resonance frequencies from Eq. 4. (**F** and **G**) Associated x-y plane dilatation fields at the first two resonances together with dilatation-amplitude line plots sampled in the y direction averaged over the interface of the input block in the area delimited by the black dashed lines (ignoring the protrusions). All dimensions are in nanometers. The color scales for each image are the same in (B) to (D) and in (F) and (G).

spectrum η(f) when no grooves are on the blocks. Resonant peaks occur at integral multiples of 46.5 GHz. By analogy with the theory of organ pipe resonances, we may write (*26*)

$$f_n = \frac{n v_e}{2L'} \qquad (2)$$

where integer n is the FP resonance mode order of the lowest-order radial modes in the nanowire and $v_e = 4320$ m s^{-1} is the velocity of extensional acoustic waves in tungsten (see Materials and Methods) (*27*). Flexural waves are precluded as a result of the chosen cylindrical symmetry. As with the case of air-filled open pipes, we use a corrected length $L' = L + 2\Delta L$, analogous to the standard in-fluid Rayleigh correction (*28, 29*) that accounts for the extra mass set in vibrational motion outside the nanowire ends. For the case of our nanowire aspect ratio $L/a = 16$, we find $\Delta L = 1.26a$, where $a = d/2$ is the nanowire radius. The frequencies f_n predicted in this way agree well with the simulations (see vertical dashed lines in Fig. 2A). Similar values of $\Delta L \sim 1.2a$ are found for $10 \leq L/a \leq 30$ (see the Supplementary

Materials). This is significantly larger than the equivalent case of open flanged pipes for which $\Delta L = 0.85a$ for $\lambda/2\pi \gg a$ (*25*).

The velocity of bulk longitudinal waves [$v_l = 5410$ m s^{-1} for tungsten (*27*)] is larger than that inside the nanowire, and mode conversion to shear and surface waves occurs at the ends, which make evaluating ΔL more complicated. Boucher and Kolsky (*30*) have shown that for an isotropic rod in frictionless contact with a half-space, the acoustic reflection coefficient depends on the aspect ratio L/a, v_e, v_l, and Poisson's ratio ν [considered here for tungsten to be 0.35 from (*27*)]. By calculating the acoustic phase change on reflection inside the nanowire, one can determine the end correction from the equation

$$\Delta L = -\frac{v_e}{2\omega} \arg(R) \qquad (3)$$

where R is the complex acoustic reflection coefficient for extensional sound waves of angular frequency ω (see details in the Supplementary Materials).
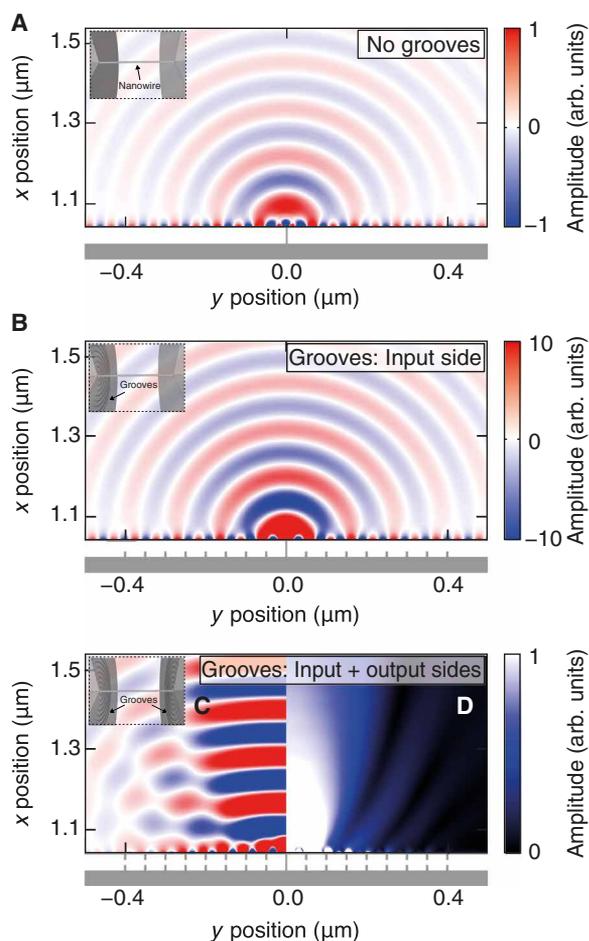
Fig. 3. Comparison of the acoustic output fields for three geometries. Dilatation fields at the first resonance on the nanowire output side. (**A**) Case of no grooves. (**B**) With $N = 8$ grooves on the input side. The groove dimensions are optimized to enhance the transmission efficiency of the first resonance. (**C**) For $N = 8$ grooves on both sides, with groove dimensions unchanged. The color scale of (C) is the same as that for (B). (**D**) Fourier modulus of the dilatation. The corresponding structure is shown to scale beneath each plot; the insets show three-dimensional views.

We derive from this theory an end correction $\Delta L = 1.40a$ for $L/a = 16$, greater than the simulation value. This disparity holds true over a wide range of aspect ratios L/a from 8 to 30 (see fig. S1) (*28, 31*)]. However, in our case, the rod is connected to two half-spaces rather than being in frictionless contact, resulting in a stiffer end condition. This raises the resonant frequency and lowers ΔL, as observed. The end correction for the solid case is important for understanding resonances in nanowires and nanorods (*32–34*) and thermal conduction therein (*35*). Apart from the frequency f_1, the associated quality factor $Q = 14$ also depends on the reflection coefficient inside the nanowire (see the Supplementary Materials) (*36*).

The resonances in the nanowire and transmitted waves can be visualized from x-y plane dilatation fields and x-direction amplitude profiles shown for each resonance in Fig. 2 (B to D) and from the field plot of Fig. 3A. This solid-state reincarnation of a free-free boundary condition at the open ends of a flanged pipe gives rise to antinodes at the extremities, visible in the images. Spherical radiation, surface waves, and the presence of intense acoustic fields

just outside the nanowire ends are also evident. A maximum transmission efficiency η just greater than 1.5 is obtained on resonance $n = 1$ (corresponding to approximately half an acoustic wavelength over the nanowire length), only barely classifying as extraordinary transmission.

Grooves on the input side
Concentric grooves on the input side are expected to enhance transmission (*12–15*) because leaky surface-guided modes in the fluid, referred to as spoof surface acoustic waves (*37*), help concentrate resonant acoustic energy through the aperture. In the present case, the grooves are expected to play an equivalent role by mode converting longitudinal waves to surface acoustic waves guided in the solid in the region of the grooves, thereby channeling more acoustic energy through the nanowire, although this has never been tested. By analogy to the fluid-solid case (*12, 13*), resonances are introduced at frequencies approximately given by

$$f_{Gm} = \frac{mv_R}{p} \tag{4}$$

where p is the groove pitch, integer m is the mode number, and $v_R = 2470 \text{ m s}^{-1}$ is the Rayleigh wave velocity on a flat tungsten surface (see Materials and Methods). The groove geometry is optimized for maximum η at $m = n = 1$ when $f_{G1} = f_1$, with $N = 8$ grooves, obtained by tuning each geometrical parameter depicted in Fig. 1E: pitch (p), width (w), height (h), and first groove position (q) (see the Supplementary Materials).

The spectrum $\eta(f)$ plotted in Fig. 2E is obtained with the optimized parameters $p = 50$ nm, $w = 6$ nm, $h = 14$ nm, and $q = 44$ nm and again shows a series of peaks, the first peak still lying at 46.5 GHz. Also shown for the first two resonances in Fig. 2 (F) and (G) are the x-y plane dilatation fields and y direction amplitude profiles, clearly revealing the marked effect of the surface acoustic wave resonances. Maximum η corresponds to $m = 1$ in Eq. 4, which predicts $f_{G1} = 49.4$ GHz (see vertical dotted line in Fig. 2B). Surface-wave acoustic dispersion induced by the periodic concentric groove array accounts for the slight difference with the simulated frequency and also for the split second and third resonances (*38*).

The grooves lead to a marked enhancement in η by a factor of ~330 and to the giant efficiency η ≈ 500 for $n = m = 1$. This is considerably larger than previous best values ~100 obtained in acoustics (*12, 18, 19*) and optics (*11*). The acoustic energy density inside the nanowire is enhanced by factor of 14,100 (see the Supplementary Materials for details of the calculation) (*39*). The value η ≈ 500 corresponds to squeezing the longitudinal acoustic energy incident on the system over a diameter of ~112 nm through the nanowire with a diameter of 5 nm equal to λ/23, where λ = 116 nm. This high acoustic concentration is a promising result for future solid-state applications, such as nanoparticle detection or imaging beyond the diffraction limit. Increasing the number of grooves N continues to give an improvement in η on first resonance up to the maximum of $N = 14$ investigated, at which point the value η = 650 is reached (see the Supplementary Materials).

Grooves on both the input and output sides
A modified output acoustic field results from additional grooves being present on the output side (*12, 14, 40*), as shown in Fig. 1D. Acoustic fields for the three geometries considered are shown in Fig. 3. The addition of grooves on the output side results in mode conversion
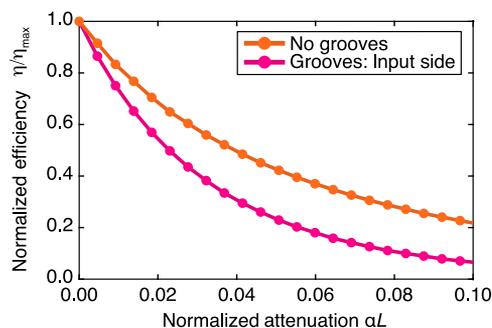
Fig. 4. Effect of ultrasonic attenuation on the transmission efficiency. Plots of the normalized efficiency η/η_{max} as a function of the normalized attenuation αL, where L is the length of the nanowire. Cases of no grooves and with $N = 8$ grooves on the input side are shown. The groove dimensions are optimized to enhance the transmission efficiency of the first resonance.

from surface acoustic waves to longitudinal waves, their coherent superposition giving rise to diffraction lobes. The result is a directed beam of longitudinal waves traveling axially, as is evident in the image in Fig. 3D, representing the modulus of the temporal Fourier transform of the dilatation. Animations of the EAT at the first resonance and in the time domain in the three cases can be viewed in Supplementary Movies. This axial concentration of longitudinal acoustic energy inside a solid should prove invaluable for acoustic wave concentration on the nanoscale in sensor applications such as single-nanoparticle detection.

DISCUSSION
So far, we have ignored the effects of ultrasonic attenuation. Figure 4 shows a plot of the simulated normalized efficiency η/η_{max} at the $n = 1$ resonance in the cases with and without grooves on the input side as a function of the ultrasonic attenuation αL of the nanowire and block material, where α is the ultrasonic attenuation coefficient and η_{max} is the value of η for $\alpha = 0$. (In the calculation of η, account is taken of the effect of wave propagation from the source to the nanowire input and from the nanowire output to the sampling region. The case of grooves on both the input and output sides is expected to be very similar to that of grooves on the input side.) η monotonically decreases with increasing αL with and without the inclusion of grooves and somewhat faster in the former case owing to the extra surface wave attenuation on multiple reflection by the grooves. For $\alpha L > 0.023$ in the case of grooves on the input side, η decreases by more than a factor of 2. For the $n = m = 1$ resonance at ~50 GHz in tungsten, at which frequency $\alpha = 1.3 \, \mu m^{-1}$ (*41*), we predict a decrease in η by a factor of ~4.7 compared to the case of no attenuation, yielding $\eta \approx 110$. However, our results are perfectly scalable to larger dimensions for which ultrasonic attenuation would be negligible at this resonance. Moreover, crystals such as silicon, as used in (*22*) for surface wave extraordinary transmission, would have negligible ultrasonic attenuation at room temperature for the present nanowire dimensions (*42*).

In conclusion, we have investigated the EAT of bulk acoustic waves confined inside a solid structure. The case of a tungsten meta-atom consisting of a subwavelength diameter solid cylinder connecting two solid tungsten half spaces is found to transmit more longitudinal acoustic energy than that predicted by geometrical considerations alone, producing EAT with efficiency $\eta \approx 1.5$ at the first

FP extensional resonance in the absence of ultrasonic attenuation. Eight concentric grooves of optimized dimension and position on the input surface that tune the first surface wave resonance to the first extensional resonance give rise to a transmission efficiency enhanced by a factor of ~330 compared to the case with no grooves, yielding the giant value $\eta \approx 500$, with further enhancement up to $\eta \sim 650$ shown to be possible by increasing the number of grooves. This unprecedented behavior is unexpected in the sense that bulk longitudinal waves in solids suffer from extra losses owing to conversion of energy on scattering to shear waves. However, despite this, the result we find is a record, giant transmission enhancement. It may even be possible to achieve future efficiency increases by changing the material or adding a cavity to the cylinder (*22*). Our results were obtained for a nanowire with a diameter of 5 nm at ~50 GHz and $\lambda \sim 120$ nm, although, as mentioned above, the results are scalable to larger dimensions and lower frequency ranges for which ultrasonic attenuation is negligible. These results should therefore also be of importance for isotropic or anisotropic solid-state geometries designed for the kilohertz-megahertz regime, leading to applications in millimeter to micron-scale acoustic transduction, sensing, and metamaterials. We fully expect that our predictions would be easier to verify with rods of centimeter order in length with the $n = m = 1$ resonance. At the same time, it would also be interesting to investigate whether incident shear waves, which would couple to flexural waves in the rod, also show extraordinary transmission.

However, nanoscale gigahertz-terahertz applications are particularly abundant. Knowledge of the Rayleigh end correction for solid rods should be useful in interpreting results for nanoresonators and in nanometrology applications based on vibrating rods with embedded ends. The inclusion of grooves on the output side may allow the concentration of more energy into acoustic resonant tips for dynamic atomic force microscopy (*43*), thereby increasing their sensitivity, or may allow the enhancement of thermal phonon transfer in nanoscale cylindrical geometries (*35*, *44*). In addition, by the use of arrays of nanowires, one could construct acoustic meta-surfaces with nanoscale structure that show extraordinary transmission. Lastly, the extreme colocalization of optical and acoustic waves in dielectric or plasmonic nanowires by dual acoustic and optical high-efficiency extraordinary transmission may lead to novel methods for nanoscale acousto-optic modulation.

MATERIALS AND METHODS
Time-domain finite element method simulations are carried out with the commercial software package PZFlex (Weidlinger Associates Inc.), exploiting the axial symmetry of rotation about the x axis. Acoustic excitation is achieved with a disc-shaped broadband pulsed source with a diameter of 800 nm (blue region in Fig. 1A) that emits plane longitudinal waves in the $+x$ direction at normal incidence on the nanowire. We used an impulsive force in the y-z plane at 600 nm from the nanowire in the x direction consisting of a half cycle of a sinusoid with a frequency of 100 GHz equally distributed over the y-z plane. Absorbing boundary conditions are applied to the lateral and horizontal boundaries. Regions outside the solid structure are assumed to be vacuum. A total of 270 frames are analyzed over a simulation time of 0.6 ns (corresponding to a temporal step of ~2.2 ps). The duration of this simulation time is sufficient for the on-resonance response sampled in the output regions to be significantly attenuated

(see the Supplementary Materials). The element size along the *x* and *y* axes is 1.1 nm (corresponding to the use of ~40 nodes per wavelength at 120 GHz for the case of longitudinal waves). This results in approximately four elements across the nanowire diameter. Trials with different element sizes suggest that the simulation accuracy at this element size is ~5%.

The density, longitudinal sound velocity, and shear velocity of tungsten are taken as their bulk values $\rho = 19{,}200 \text{ kg m}^{-3}$, $v_l = 5410 \text{ m s}^{-1}$, and $v_t = 2640 \text{ m s}^{-1}$, respectively (*27*). Any changes in modulus owing to decreasing dimensional scale are ignored. The velocity of extensional waves $v_e = 4320 \text{ m s}^{-1}$ is obtained from $v_e = \sqrt{E/\rho}$, where E is the Young's modulus (which can be found with a knowledge of v_l and v_t, since tungsten is effectively isotropic) (*26*). At our values of $\lambda/d \sim 20$, dispersive effects from radial inertia are negligible (*26*). The Rayleigh wave velocity $v_R = 2470 \text{ m s}^{-1}$ can be calculated from the analytical expression (*26*) $v_R = v_t(0.87 + 1.12v)/(1 + v)$.

To estimate the longitudinal wave energy transmitted, we analyze the elastic dilatation $\delta = \varepsilon_{xx} + \varepsilon_{yy} + \varepsilon_{zz}$, where $\varepsilon_{xx,yy,zz}$ are the longitudinal strain components (*45*) along the *x*, *y*, and *z* axes, respectively, as shown in Fig. 1A. The presence of surface waves on the output face only have a minor influence (<10%) on the calculation of $\eta(f)$. A detailed description of the analysis regions is given in the Supplementary Materials.

SUPPLEMENTARY MATERIALS

REFERENCES AND NOTES

1. C. Genet, T. W. Ebbesen, Light in tiny holes. *Nature* **445**, 39–46 (2007).
2. T. W. Ebbesen, H. J. Lezec, H. Ghaemi, T. Thio, P. Wolff, Extraordinary optical transmission through sub-wavelength hole arrays. *Nature* **391**, 667–669 (1998).
3. X. Zhang, Acoustic resonant transmission through acoustic gratings with very narrow slits: Multiple-scattering numerical simulations. *Phys. Rev. B* **71**, 241102 (2005).
4. M.-H. Lu, X.-K. Liu, L. Feng, J. Li, C.-P. Huang, Y.-F. Chen, Y.-Y. Zhu, S.-N. Zhu, N.-B. Ming, Extraordinary acoustic transmission through a 1D grating with very narrow apertures. *Phys. Rev. Lett.* **99**, 174301 (2007).
5. B. Hou, J. Mei, M. Ke, W. Wen, Z. Liu, J. Shi, P. Sheng, Tuning fabry-perot resonances via diffraction evanescent waves. *Phys. Rev. B* **76**, 054303 (2007).
6. L. Zhou, G. A. Kriegsmann, Complete transmission through a periodically perforated rigid slab. *J. Acoust. Soc. Am.* **121**, 3288–3299 (2007).
7. J. Christensen, L. Martin-Moreno, F. J. Garcia-Vidal, Theory of resonant acoustic transmission through subwavelength apertures. *Phys. Rev. Lett.* **101**, 014301 (2008).
8. H. Estrada, P. Candelas, A. Uris, F. Belmar, F. J. García de Abajo, F. Meseguer, Extraordinary sound screening in perforated plates. *Phys. Rev. Lett.* **101**, 084302 (2008).
9. T. Thio, K. Pellerin, R. Linke, H. Lezec, T. Ebbesen, Enhanced light transmission through a single subwavelength aperture. *Opt. Lett.* **26**, 1972–1974 (2001).
10. F. J. García-Vidal, H. J. Lezec, T. W. Ebbesen, L. Martín-Moreno, Multiple paths to enhance optical transmission through a single subwavelength slit. *Phys. Rev. Lett.* **90**, 213901 (2003).
11. O. T. A. Janssen, H. P. Urbach, G. W. 't Hooft, Giant optical transmission of a subwavelength slit optimized using the magnetic field phase. *Phys. Rev. Lett.* **99**, 043902 (2007).
12. J. Christensen, A. I. Fernandez-Dominguez, F. de Leon-Perez, L. Martin-Moreno, F. J. Garcia-Vidal, Collimation of sound assisted by acoustic surface waves. *Nat. Phys.* **3**, 851–852 (2007).
13. Y. Zhou, M.-H. Lu, L. Feng, X. Ni, Y.-F. Chen, Y.-Y. Zhu, S.-N. Zhu, N.-B. Ming, Acoustic surface evanescent wave and its dominant contribution to extraordinary acoustic transmission and collimation of sound. *Phys. Rev. Lett.* **104**, 164301 (2010).
14. J. Mei, B. Hou, M. Ke, S. Peng, H. Jia, Z. Liu, J. Shi, W. Wen, P. Sheng, Acoustic wave transmission through a bull's eye structure. *Appl. Phys. Lett.* **92**, 124106 (2008).
15. Z.-B. Li, Y.-H. Yang, X.-T. Kong, W.-Y. Zhou, J.-G. Tian, Fabry–perot resonance in slit and grooves to enhance the transmission through a single subwavelength slit. *J. Opt. A Pure Appl. Opt.* **11**, 105002 (2009).
16. N. Aközbek, N. Mattiucci, M. J. Bloemer, M. Sanghadasa, G. D'Aguanno, Manipulating the extraordinary acoustic transmission through metamaterial-based acoustic band gap structures. *Appl. Phys. Lett.* **104**, 161906 (2014).
17. S. Carretero-Palacios, A. R. J. Murray, L. Martín-Moreno, A. P. Hibbins, Broadband and broadangle extraordinary acoustic transmission through subwavelength apertures surrounded by fluids. *New J. Phys.* **16**, 083044 (2014).
18. R. Fleury, A. Alù, Extraordinary sound transmission through density-near-zero ultranarrow channels. *Phys. Rev. Lett.* **111**, 055501 (2013).
19. J. J. Park, K. J. B. Lee, O. B. Wright, M. K. Jung, S. H. Lee, Giant acoustic concentration by extraordinary transmission in zero-mass metamaterials. *Phys. Rev. Lett.* **110**, 244302 (2013).
20. V. Koju, E. Rowe, W. M. Robertson, Extraordinary acoustic transmission mediated by helmholtz resonators. *AIP Adv.* **4**, 077132 (2014).
21. B. C. Crow, J. M. Cullen, W. W. McKenzie, V. Koju, W. M. Robertson, Experimental realization of extraordinary acoustic transmission using Helmholtz resonators. *AIP Adv.* **5**, 027114 (2015).
22. S. Mezil, K. Chonan, P. H. Otsuka, M. Tomoda, O. Matsuda, S. H. Lee, O. B. Wright, Extraordinary transmission of gigahertz surface acoustic waves. *Sci. Rep.* **6**, 33380 (2016).
23. B. Wu, A. Heidelberg, J. J. Boland, Mechanical properties of ultrahigh-strength gold nanowires. *Nat. Mater.* **4**, 525–529 (2005).
24. X. L. Feng, R. He, P. Yang, M. L. Roukes, Very high frequency silicon nanowire electromechanical resonators. *Nano Lett.* **7**, 1953–1959 (2007).
25. S. N. Raja, R. Rhyner, K. Vuttivorakulchai, M. Luisier, D. Poulikakos, Length scale of diffusive phonon transport in suspended thin silicon nanowires. *Nano Lett.* **17**, 276–283 (2017).
26. K. Graff, *Wave Motion in Elastic Solids, Dover Books on Engineering Series* (Dover Publications, 1975).
27. D. E. Gray, *American Institute of Physics Handbook* (McGraw-Hill, 1982).
28. L. Rayleigh, *The Theory of Sound* (Dover, 1945), vol. 2, pp. 180–183.
29. D. T. Blackstock, *Fundamentals of Physical Acoustics* (John Wiley & Sons, 2000).
30. S. Boucher, H. Kolsky, Reflection of pulses at the interface between an elastic rod and an elastic half-space. *J. Acoust. Soc. Am.* **52**, 884 (1972).
31. D. A. Spence, The hertz contact problem with finite friction. *J. Elasticity* **5**, 297–319 (1975).
32. S. V. Goupalov, Crystal structure anisotropy explains anomalous elastic properties of nanorods. *Nano Lett.* **14**, 1590–1595 (2014).
33. Y. Gan, C. Wang, Z. Chen, Ultrafast laser-excited vibration and elastic modulus of individual gold nanorods. *Opt. Lett.* **40**, 340–343 (2015).
34. M. Hu, X. Wang, G. V. Hartland, P. Mulvaney, J. P. Juste, J. E. Sader, Vibrational response of nanorods to ultrafast laser induced heating: Theoretical and experimental analysis. *J. Am. Chem. Soc.* **125**, 14925–14933 (2003).
35. R. Prasher, T. Tong, A. Majumdar, An acoustic and dimensional mismatch model for thermal boundary conductance between a vertical mesoscopic nanowire/nanotube and a bulk substrate. *J. Appl. Phys.* **102**, 104312 (2007).
36. B. E. Saleh, M. C. Teich, *Fundamentals of Photonics* (John Wiley & Sons, 2019).
37. Y. Ye, M. Ke, Y. Li, T. Wang, Z. Liu, Focusing of spoof surface-acoustic-waves by a gradient-index structure. *Appl. Phys.* **114**, 154504 (2013).
38. N. E. Glass, R. Loudon, A. A. Maradudin, Propagation of rayleigh surface waves across a large-amplitude grating. *Phys. Rev. B* **24**, 6843 (1981).
39. P. H. Otsuka, K. Nanri, O. Matsuda, M. Tomoda, D. M. Profunser, I. A. Veres, S. Danworaphong, A. Khelif, S. Benchabane, V. Laude, O. B. Wright, Broadband evolution of phononic-crystal-waveguide eigenstates in real- and k-spaces. *Sci. Rep.* **3**, 3351 (2013).
40. J. Cui, J. Liu, Y. Mao, Y. Li, X. Liu, Realization of manipulating acoustic surface waves radiation direction with rectangular-groove structure. *AIP Adv.* **7**, 115301 (2017).
41. O. Matsuda, M. Tomoda, T. Tachizaki, S. Koiwa, A. Ono, K. Aoki, R. P. Beardsley, O. B. Wright, Ultrafast ellipsometric interferometry for direct detection of coherent phonon strain pulse profiles. *J. Opt. Soc. Am. B* **30**, 1911–1921 (2013).

42. B. C. Daly, K. Kang, Y. Wang, D. G. Cahill, Picosecond ultrasonic measurements of attenuation of longitudinal acoustic phonons in silicon. *Phys Rev. B* **80**, 174112 (2009).

43. B. D. Huey, AFM and acoustics: Fast, quantitative nanomechanical mapping. *Annu. Rev. Mat. Res.* **37**, 351–385 (2007).

44. C. Jean, L. Belliard, T. W. Cornelius, O. Thomas, M. E. Toimil- Molares, M. Cassinelli, L. Becerra, B. Perrin, Direct observation of gigahertz coherent guided acoustic phonons in free-standing single copper nanowires. *J. Phys. Chem. Lett.* **5**, 4100–4104 (2014).

45. O. Matsuda, M. C. Larciprete, R. L. Voti, O. B. Wright, Fundamentals of picosecond laser ultrasonics. *Ultrasonics* **56**, 3–20 (2015).

Citation: T. Devaux, H. Tozawa, P. H. Otsuka, S. Mezil, M. Tomoda, O. Matsuda, E. Bok, S. H. Lee, O. B. Wright, Giant extraordinary transmission of acoustic waves through a nanowire. *Sci. Adv.* **6**, eaay8507 (2020).

Science Advances

Giant extraordinary transmission of acoustic waves through a nanowire

T. Devaux, H. Tozawa, P. H. Otsuka, S. Mezil, M. Tomoda, O. Matsuda, E. Bok, S. H. Lee and O. B. Wright

ARTICLE TOOLS	http://advances.sciencemag.org/content/6/10/eaay8507
SUPPLEMENTARY MATERIALS	http://advances.sciencemag.org/content/suppl/2020/03/02/6.10.eaay8507.DC1
REFERENCES	This article cites 40 articles, 0 of which you can access for free http://advances.sciencemag.org/content/6/10/eaay8507#BIBL
PERMISSIONS	http://www.sciencemag.org/help/reprints-and-permissions

Use of this article is subject to the Terms of Service